Ammonia and methane emissions from dairy concentrated animal feeding operations in California, using mobile optical remote sensing

Vechi, N.T.; Mellqvist, J.; Samuelsson, J.; Offerle, B.; Scheutz, C.

Published in:
Atmospheric Environment

Link to article, DOI:
10.1016/j.atmosenv.2022.119448

Publication date:
2023

Document Version
Publisher's PDF, also known as Version of record

Atmospheric Environment 293 (2023) 119448

Contents lists available at ScienceDirect

Atmospheric Environment

journal homepage: www.elsevier.com/locate/atmosenv

Ammonia and methane emissions from dairy concentrated animal feeding operations in California, using mobile optical remote sensing

N.T. Vechi [a,b,*], J. Mellqvist [a], J. Samuelsson [c], B. Offerle [c], C. Scheutz [b]

[a] Department of Space, Earth and Environment, Chalmers University of Technology, Göteborg, Sweden
[b] Department of Environmental and Resource Engineering, Technical University of Denmark, 2800 Kgs, Lyngby, Denmark
[c] FluxSense AB, SE-41296, Göteborg, Sweden

HIGHLIGHTS

- NH_3 and CH_4 emissions were quantified using direct and indirect flux methods.
- NH_3 and CH_4 emission factors averaged 9.1 g_{NH3}/LU/h and 40.1 g_{CH4}/LU/h.
- Day-time NH_3 emission factors were 28% higher than estimated by NEI 2014.
- Quantified CH_4 emission factors were 60% higher than the CARB inventory.

ARTICLE INFO

Keywords:
CAFO
SOF
Dairy
Emission inventory
Emission factor

ABSTRACT

Dairy concentrated animal feeding operations (CAFOs) are significant sources of methane (CH_4) and ammonia (NH_3) emissions in the San Joaquin Valley, California. Optical techniques, namely, remote sensing by Solar Occultation Flux (SOF) and Mobile extractive FTIR (MeFTIR), were used to measure NH_3 air column and ground air concentrations of NH_3 and CH_4, respectively. Campaigns were performed in May and October 2019 and covered 14 dairies located near Bakersfield and Tulare, California. NH_3 and CH_4 emission rates from single CAFOs averaged 101.9 ± 40.6 kg_{NH3}/h and 437.7 ± 202.0 kg_{CH4}/h, respectively, corresponding to emission factors (EFs) per livestock unit of 9.1 ± 2.7 g_{NH3}/LU/h and 40.1 ± 17.8 g_{CH4}/LU/h.

The NH_3 emissions had a median standard uncertainty of 17% and an expanded uncertainty (95% Confidence Interval (CI)) of 37%; meanwhile, CH_4 emissions estimates had greater uncertainty, median of 25% and 53% (in the 95% CI). Decreasing NH_3 to CH_4 ratios and NH_3 EFs from early afternoon (13:00) to early night (19:00) indicated a diurnal emission pattern with lower ammonia emissions during the night. On average, measured NH_3 emissions were 28% higher when compared to daytime emission rates reported in the National Emissions Inventory (NEI) and modeled according to diurnal variation. Measured CH_4 emissions were 60% higher than the rates reported in the California Air Resources Board (CARB) inventory. However, comparison with airborne measurements showed similar emission rates. This study demonstrates new air measurement methods, which can be used to quantify emissions over large areas with high spatial resolution and in a relatively short time period. These techniques bridge the gap between satellites and individual CAFOs measurements.

1. Introduction

The quantification and monitoring of ammonia (NH_3) and methane (CH_4) emission sources are crucial to effectively plan and implement air quality and climate change policies. CH_4 is a potent greenhouses gas and has a global warming potential of 27 over a 100-year span (IPCC, 2021). NH_3 is a critical precursor of fine particulate matter ($PM_{2.5}$), which has implications for human health and climate change (Lelieveld et al., 2015). In addition, atmospheric NH_3 can be transported to downwind ecosystems leading to eutrophication and loss of biodiversity (Harris et al., 2016). Livestock operations are large emission sources of both NH_3 and CH_4, and in California, the agricultural sector contributes 8% of total GHG emissions and approximately 57% of the state's anthropogenic CH_4 emissions (CARB, 2019a). For NH_3, livestock operations are

* Corresponding author. Department of Space, Earth and Environment, Chalmers University of Technology, Göteborg, Sweden.
E-mail address: navei@dtu.dk (N.T. Vechi).

https://doi.org/10.1016/j.atmosenv.2022.119448
Received 24 June 2022; Received in revised form 20 October 2022; Accepted 24 October 2022
Available online 29 October 2022

responsible for 56% of total emissions in California (U.S. Environmental protection Agency, 2018). These numbers are a reflection of the state's number one ranking, as the largest milk producer in the USA, with production concentrated in the San Joaquin Valley (SJV) (Monson et al., 2017; USDA, 2021). However, these estimates have large uncertainties, and better understanding of NH_3 and CH_4 emissions from livestock operations can facilitate policymaking for achieving California's air quality and climate goals. Concentrated animal feeding operations (CAFOs) are defined as operations where animals are confined for a certain amount of time and where vegetation is not sustained, additionally, they should meet the requirement of more than 700 milk cows (US-EPA, 2012).

NH_3 emissions from livestock originate from the mixture of animal urine and feces, and they are highly variable and depend on a number of factors such as temperature, pH, wind speed, manure composition, and manure management (Hristov et al., 2011). Shortly, nitrogen molecules in the manure are converted to NH_3, which stays in equilibrium with its ionized form ammonium (NH_4^+). In favorable conditions NH_3 is transported to the manure surface by diffusion and further volatilized from the manure surface by convection (Hristov et al., 2011). NH_3 lifetime in the atmosphere varies from hours to a few days according to atmosphere composition. In Palm Springs (California) for example, the load of oxidants reduced NH_3 life time to four to six hours (Leifer et al., 2017). Part of the NH_3 emitted reacts neutralizing acid species as H_2SO_4 and HNO_3 forming $PM_{2.5}$, during the San Joaquin Valley (SJV) episodes of high particulate concentrations occuring specially in the winter (Lonsdale et al., 2017). Moreover, the NH_3 left is deposited on soil and water surfaces. Miller et al. (2015) measured a ~30% decrease in the ratio of NH_3:CH_4 within a few kilometers of a dairy facility in the SJV and attributed the difference to NH_3 deposition. Overall the modeling and understanding of NH_3 dynamics is a complex task having to account for all the mechanism mentioned above (Lonsdale et al., 2017; Zhu et al., 2015b). On the other hand, CH_4 emissions from dairy operations come from both manure management and enteric fermentation, with emissions from the latter depending mainly on animal age, feed intake, and body weight (Hristov et al., 2018), while emissions from manure are affected by temperature and management practices (Rennie et al., 2018). Furthermore, emissions might have a diurnal trend associated with wind speed, temperature, and cattle activity (Leytem et al., 2011). Although many studies (Leytem et al., 2011; Sun et al., 2015) show a clear diurnal pattern for NH_3, the same is not true for CH_4, which provide contradictory results (Arndt et al., 2018; Bjorneberg et al., 2009; Golston et al., 2020).

Direct emissions quantification offers information that can be used to improve inventories, evaluate emission dynamics, and determine the efficiency of different mitigation strategies. Several studies in North America show that inventories have lower emissions estimations than measurements of both NH_3 (Lonsdale et al., 2017; Nowak et al., 2012) and CH_4 (Hristov et al., 2017; Miller et al., 2013; Owen and Silver, 2015), while others reveal good agreement (Arndt et al., 2018; Golston et al., 2020).

The solar occultation flux (SOF) technique has been used to measure industrial emissions for about 20 years, with most studies focusing on VOCs (alkanes and alkenes) (Johansson et al., 2014; Mellqvist et al., 2010) and industrial NH_3 (Mellqvist et al., 2007). NH_3 measurements of dairy and beef farms using the SOF technique have been carried out by Kille et al. (2017) in Colorado. Mass fluxes can be obtained by combining wind information and the path-integrated concentrations retrieved from the gas columns of solar spectra collected by the SOF instrument on a moving measurement platform. The technique can be used to study emissions from single-point sources to larger areas (radius ~ 50 km), and it can therefore help to fill gaps between point concentration measurements and satellite remote sensing.

In this study, SOF together with local wind profile measurements were used to measure NH_3 emissions from CAFOs. In addition, CH_4 measurements were carried out via an emission ratio approach, combining direct NH_3 flux measurement by SOF with plume NH_3 to CH_4 concentration ratios. The aim of this study was threefold. First CH_4 and NH_3 emissions were investigated from several individual dairy CAFOs located at the SJV. These facilities were selected according to measurements possibilities with respect to wind direction and drivable roads and due to their large size. Results were then evaluated by comparing them with the inventory estimates and other reports in the literature. Lastly, the causes of variability in the NH_3 emission factors obtained were identified and discussed.

2. Methodology

2.1. CAFOs and measurement campaigns

The study focused on emissions from dairy concentrated animal feeding operations (CAFOs) in the SJV, California. The first campaign took place in May 2019 and consisted of 11 measurement days, while the second took place in October 2019, lasting five days. In May, CAFOs were measured in Kern (near Bakersfield) and Tulare Counties, whereas in October, only the facilities in Kern County were revisited.

In the application of the SOF method for industrial measurements (European standard 2022, EN 17628:2022) there are quality criteria for the measurements to be valid. In this study we have used a subset of these, given that animal operations are less complex than industries, including that at least four plume transects need to be carried out on a single day and that the wind speed is higher than 1.5 m/s. In total, emissions from 14 individual dairy CAFOs passed the quality control requirements. Table 1 provides an overview of the facilities measured, including information on numbers of animals as well as manure management (Fig. 1c). Emission factors (EFs) were calculated by normalizing the measured emission rates by livestock units (LU) based on animal body weight, with one LU equaling 500 kg (Ngwabie et al., 2011). Although emission measurements were also successful at two facilities in Madera County in May, they were excluded from the EFs and inventory analysis since the numbers of animals were unavailable for them, but a comparison of their emissions rates with other studies is shown in section 4.3.2. All the CAFOs stored the manure in anaerobic

Table 1
CAFOs characteristics. The CAFOs are named according to their geographic location (Fig. 1c), whereby the first letter corresponds to the cardinal direction (North, South, West, East) and the second letter to the nearby city (Bakersfield (Kern County) or Tulare).

CAFOs	Mature cows[a]	Heifers and bulls	Calves	Livestock unit[b]	Covered lagoon and gas collection
SB2	7380	13414	2880	21626	No
SB3	6450	6280	1300	14184	Yes
SB4	4000	2358	0	7361	No
SB5	8115	2100	0	12749	No
NB1	5250	3620	0	10056	No
NB2	6640	1925	0	10592	No
WT1	11350	8870	0	14883	Yes
WT3	12100	0	925	12618	No
WT4	9980	2060	0	15241	No
WT5	3075	3600	0	7111	Yes
WT6	4820	4620	0	10308	No
WT7	2770	2135	0	5503	Yes
ET1	1375	1000	0	2678	No
ET8	10900	5000	0	12368	Yes

[a] Accounting both milking and dry cows.
[b] One LU = 500 kg of body weight. Holstein dairy cow = 1.36 LU, Jersey dairy cow = 0.91 LU, Holstein heifer = 0.81 LU, Jersey heifer = 0.5, Holstein calf = 0.23 LU, Jersey calf = 0.18 LU. Body weight based on U.S. Environmental Protection Agency (2013) for Holstein, by The Pennsylvania State University (2017) for heifers and calves, and American Jersey Cattle Association (2015) for mature Jersey. The numbers of mature cows, heifers, and calves at the individual farms were obtained from San Joaquin Valley Air Pollution Control District (San Joaquin Valley Air Pollution Control District, Personal Communication, 2019) and based on data from the last inspection between 2018 and 2019.

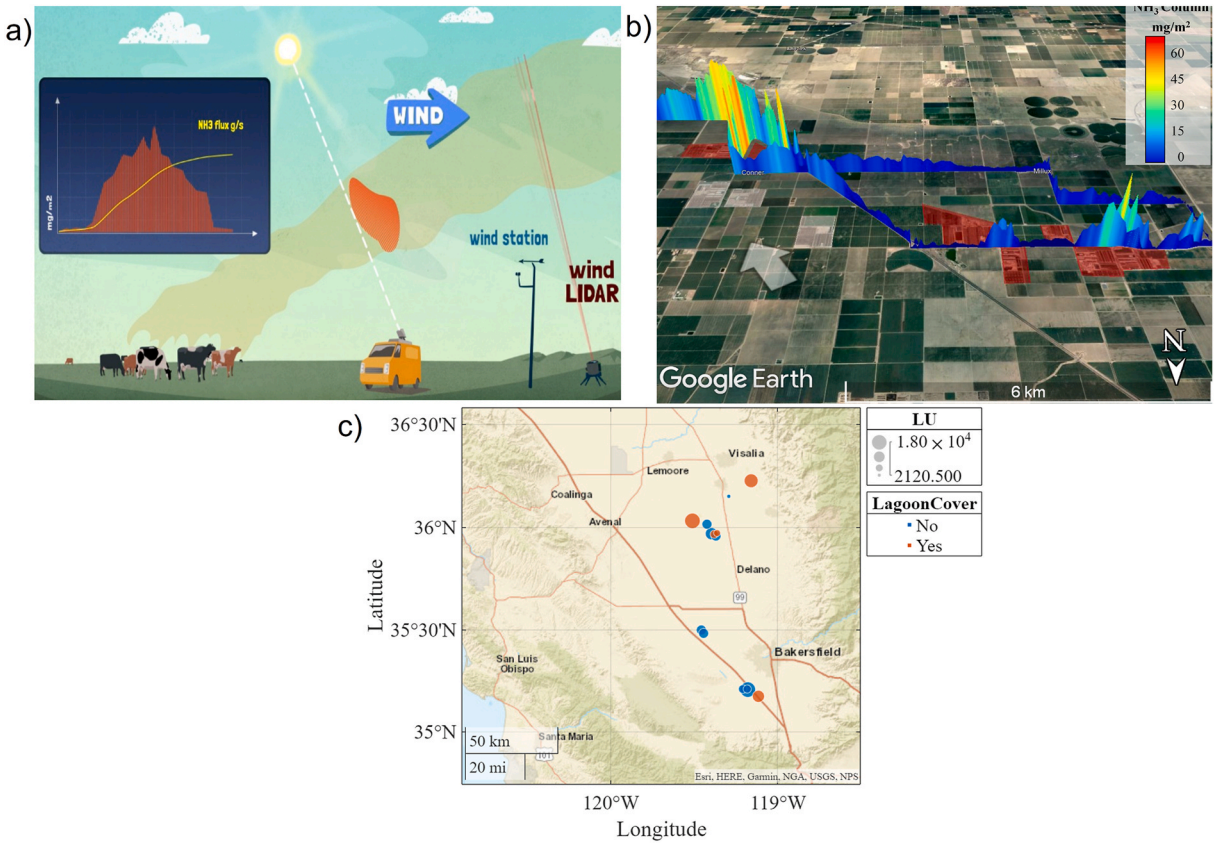

Fig. 1. (a) The principle behind the solar occultation flux (SOF) method, which was used to measure NH_3 fluxes. The car drives across the plume, measuring enhanced NH_3 concentration air columns, while the wind LIDAR is positioned close to the source and measures wind speed from 10 to 300 m high. (b) Example of SOF columns measured downwind at six facilities (red areas). The white arrow indicates the wind direction, the white shadowed areas are other farms were not measured Map source: Google Earth. (c) CAFOs location in the San Joaquin Valley, California. The size of the bubbles are proportional to the dairy size (number of animals) and the color is related to the presence of a covered lagoon (digester). (For interpretation of the references to color in this figure legend, the reader is referred to the Web version of this article.)

lagoons, and five of them had a covered lagoon, which worked as a digester, for gas collection and utilization for generation of electricity and conversion to compressed natural gas (CNG). There was some uncertainty, though, whether they were actually operational.

2.2. Measuring principles and instrumentations

CH_4 and NH_3 emissions were measured using a mobile laboratory equipped with several optical systems (Mellqvist et al., 2017). Two measurement systems were used, i.e., the solar occultation flux method (SOF), consisting of a solar tracker connected to a Fourier transform infrared spectrometer (FTIR), and a mobile extractive Fourier transform infrared (MeFTIR), consisting of an FTIR spectrometer coupled to a multireflection gas cell (Table 2). A GPS recorded the car's position while driving. Meteorological measurements were performed with (1) a sonic instrument (AIRMAR) located on the roof of the vehicle and (2) a light detection and ranging instrument (LIDAR, Zephyr) with a measurement range of 10–300 m in height and positioned close to the specific emission source (maximum distance of 5 km). The sonic sensor was only used for the operator's guidance during the measurements, while the LIDAR measurements were used for the emissions calculations (see section 2.3.3).

NH_3 columns (mg/m^2) were obtained using the solar SOF technique (Fig. 1a). In this method (Mellqvist et al., 2010), solar infrared spectra are recorded using a customized solar tracker, with mirrors reflecting the solar beam into an FTIR (Bruker IRCube), when crossing the plume concentration downwind of the emission source (Fig. S1, in Supplementary Information (SI)). The measurements do not provide the absolute atmospheric column but the differential one, relative to a reference point, usually taken outside of the plume, and a slant column of the target species is retrieved from each spectrum. The SOF retrieval uses customized analysis software (Fluxmeasure), which fits a set of spectra from the HITRAN2004 (Rothman et al., 2005) and PNNL (Sharpe et al., 2004) spectroscopic databases in a least-squares fitting procedure. The software has been tested (Kihlman, 2005) against other published codes (Griffith, 1996). The instrument incorporates a dual semi-conductor detector to increase the useable frequency range (InSb

Table 2
Summary of gas measurement techniques.

Method	Compound	Detection limit (3σ)[a]	Wind speed tolerance	Sampling time resolution	Measured quantity
SOF	NH_3	2.2 mg/m^2	1.5–12 m/s	4–5 s	Integrated vertical column mass (mg/m^2)
MeFTIR	CH_4 NH_3	30 ppbv 15 ppbv		9–10 s	Mass concentration at vehicle height (mg/m^3)

[a] The detection limit was calculated as the three times the standard deviation of constant concentration reading. These values are on the high end of the instrument limits because they were measured in field conditions, where air is not clean.

(1800–4000 cm^{-1})/MCT (700-1200 cm^{-1}). NH_3 is measured in the spectral region between 900 and 1000 cm^{-1} at a spectral resolution of 0.5 cm^{-1}, and the unique absorption features of this gas in the "fingerprint region" are advantageous in terms of specificity. More details on the instrument and validation experiments can be found in Johansson et al. (2014), Mellqvist et al. (2010), and Mellqvist et al. (2017).

CH_4 and NH_3 ground concentrations (mg/m^3) were measured using MeFTIR, in which infrared radiation from an internal glow is transmitted through an optical multi-pass measurement cell. The ambient air is pumped via an inlet placed at 2 m height through the cell at high flow (100 ml/min and cell pressure of 10 mbar below ambient pressure), to ensure that the gas volume in the cell is rapidly replaced ($t_{90} < 10$ s, gas exchange rate). The transmitted light is measured with an FTIR identical to that applied for SOF (Bruker IR Cube) (Figs. S1 and SI). Concentration retrieval of the gas species is carried out using the same spectroscopic software and databases as for SOF. NH_3 was retrieved in the same interval as in SOF (900–1000 cm^{-1}), while for CH_4 the interval used was in the C–H strength region (2760–3028 cm^{-1}). More details on the instruments and methods can be found in Samuelsson et al. (2018). The retrieval of NH_3 followed similar procedure as described for SOF while for CH_4 the retrieval was done by using the known published code, Multiple Atmospheric Layer Transmission (MALT) (Griffith, 1996).

In general, emissions were measured by driving downwind of the CAFO at a distance about hundred meters from its fenceline and this was close enough to avoid the influence of emissions from neighboring sources. Upwind measurements and the identification of external sources using GIS tools e.g., Google Earth, were used as a criterion to identify interfering emission sources (Fig. 1b). Because measurements were made by isolating the CAFOs in a box and checking upwind and downwind concentrations, interfering sources were most likely not affecting the quantification. In addition to diurnal measurements, ground concentration measurements were performed close to sunset or at night, when SOF measurements were no longer possible, this was to confirm potential variation in the NH_3:CH_4 ratio.

2.3. Emission rate calculations

2.3.1. Direct ammonia flux measurements

To obtain NH_3 emissions, the measured slant columns are first converted to vertical columns. These are subsequently integrated across the plume, corresponding to the accumulated mass across the plume (g/m). To obtain the gas flux (g/s), the accumulated mass (g/m) is multiplied by the average wind speed (m/s) of the plume (Eq. (1)). The latter applies when the plume is transected orthogonally; otherwise, the wind speed component orthogonal to the travel direction is utilized.

$$E_{NH3}\left(\frac{mg}{s}\right) = u_t\left(\frac{m}{s}\right)\int_{x1}^{x2} Column_{NH3}\left(\frac{mg}{m^2}\right) \bullet \cos(\theta) \bullet \sin(\alpha)dx(m) \quad (1)$$

where E_{NH3} is the NH_3 emission rate, u_t is the average wind speed at plume height, $column_{NH3}$ is the concentration retrieved from the solar spectrum, θ is the angle of the light path from zenith, α is the angle between the wind direction and driving direction, and x_1 and x_2 are the start- and endpoints of the plume transect, respectively. Note that because solar spectra are measured, the slant column densities will vary with latitude, season, and time of the day. The NH_3 emissions of each CAFO was calculated as the average emission of the performed transects on the respective facility.

2.3.2. Indirect CH_4 flux measurements

From MeFTIR, the ground concentrations for NH_3 and CH_4 are retrieved; hence, to quantify emissions, an indirect flux calculation approach is used. With this method, the measured concentration ratio between the two gases is combined with the gas flux measurements of one of these gases to derive the gas flux of the other one. Therefore, we combined the average NH_3:CH_4 ratio, with the average NH_3 flux obtained from SOF measurement (Eq. (1)), to find the average CAFO CH_4 emission (Eq. (2)).

$$E_{CH4} = \frac{1}{n}\sum_n E_{NH3}\left(\frac{kg}{h}\right) \Big/ \frac{1}{n}\sum_n \frac{\int_{x1}^{x2}(C_{NH3} - C_{BG-NH3})\left(\frac{\mu g}{m^3}\right)dx}{\int_{x1}^{x2}(C_{CH4} - C_{BG-CH4})\left(\frac{\mu g}{m^3}\right)dx} \quad (2)$$

Where E_{CH4} is the CH_4 emission rate, n is the number of transects and C is the concentration measured by MeFTIR. Additionally, the background concentrations ($C_{BG\text{-}NH3}$ or $C_{BG\text{-}CH4}$) were decreased from the concentrations measured when crossing the plume (C_{NH3} or C_{CH4}) Note that in this study, the SOF and MeFTIR measurements were not always carried out simultaneously, and Eq. (2) was therefore applied using average concentration ratio values and average flux values over the same time of day (from 09:00 to 17:30).

Ratio concentration measurements can be carried out with techniques other than MeFTIR, but the advantage of using the same spectroscopic approach for both column and concentration is that systematic spectroscopic errors are reduced, and there is consistency in which species are being measured. The indirect flux measurement approach relies on the assumption that the path-integrated concentration ratio of the two species is proportional to the ratio of the emissions. This means that the two species are dispersed in the same manner, requiring that they have the same release height and travel the same distance from the release point to the measurement point. NH_3 and CH_4 ground plumes were not always correlated, due to differences in the sources' location, which could lead to over- or underestimations (Delre et al., 2018; Miller et al., 2015). However, if the sources' distances to the actual road were very different in comparison to the measuring distance, the plumes were excluded, in order to avoid large under- and/or overestimations. Nevertheless, the spatial correlation was considered in the uncertainty analysis (Section 4.1).

2.3.3. Wind measurements

Local wind speed, along with its direction, is an integrated part of emission measurements (Eq. (1)), and associated uncertainties are directly propagated into the flux estimation. For the SOF method, the average wind speed of the emission plume should be used.

In this study, wind profiles close to the studied dairies were measured using wind LIDAR (LIght Detection and Ranging), i.e. a remote sensing technique, which measures wind speed by calculating the change in frequency due to the Doppler shift of the emitted laser wave (~1.5 μm) when reflected back on moving atmospheric aerosols (Locker and Woodward, 2010). The LIDAR used here (Campbell Scientific, LIDAR ZX 300) operates between 10 m and 300 m, and it is based on a continuous laser that transmits light in a 30° cone relative to zenith, combined with adaptive receiving optics that sequentially focuses on different atmospheric heights. In this study the wind speed was averaged in 5 min intervals over three height ranges, i.e. 10-50 m, 10–100 m, and 10–300 m. The accuracy of wind speed measurements is stated as 0.1 m/s, wind direction of 0.5°, and vertical precision at around 10 m. A field test comparing measurements done by cup anemometers on a 100 m wind tower to the Zephyr LIDAR showed a correlation between the two of 95% (3-week measurement period) (Smith et al., 2006).

As mentioned above, SOF measurements do not provide information on the height of the emission plume, which is of relevance when estimating average wind speed for the plume for Eq. (1). However, it is possible to estimate the plume height using vertical and horizontal wind speeds rates and distance from the measurement road to the source (Johansson, 2016). Based on previous studies in Texas (Johansson et al., 2014; Mellqvist et al., 2010) vertical dispersion rates of 0.5–1 m/s were used, which was obtained by wind soundings and aircraft measurements.

For most measurements, the wind intervals of 10–50 m and 10–100 m were found to be most appropriate for calculation of average plume wind speed, with just two exceptions. However, in reality there was only

12% difference between these two intervals since the wind variation is the strongest close to the ground and this was taken into account in the uncertainty analysis (Section 4.1).

The prevailing wind in southern San Joaquin Central Valley flows from the north/northwest direction during the day, and this was true for all measuring days in Bakersfield, when LIDAR measurements often resumed after the sunset, and the instrument was positioned at a maximum of 5 km downwind of the source. In Tulare, higher wind speeds and different directions were encountered (Fig. S2 in SI).

2.3.4. Techniques' advantages and challenges

NH_3 is a sticky gas that is easily being adsorbed on surfaces and this poses challenges for measurements using extractive techniques, and concentrations are thus easily underestimated. SOF, however, is a contact-free technique, which makes it more suitable to measure such types of gases. Other advantages of the technique lie in its capability to measure path integrated gas columns, mobility and real-time responsivity, thereby making it possible to measure multiple emission sources over a short time period. On the other hand, MeFTIR is a close-path instrument, where the adsorption of NH_3 in the cell and inlet might play a role. To minimize the adsorption on internal surfaces (Brodeur et al., 2009), which would cause a time delay in the measurements, the inlet tubing and the cell are heated to a minimum of 40 °C, thereby ensuring that NH_3 is not adsorbed inside the tubing or the measurement chamber.

Primarily, measurements of columns and ground concentrations were carried out simultaneously. However, sometimes this was not possible (25% of the time), due to very low concentrations at the ground level. SOF columns are only measured during daytime and sunny conditions (low cloud coverage), which generally is associated with strong vertical convection. However, it can be difficult to carry out ground concentration measurements during these conditions, where a better detection is often obtained after sunset.

2.4. Emission inventories

2.4.1. Ammonia emission rate comparison with the NEI 2014 inventory

The measured farm-scale NH_3 emission rates were compared to farm-specific daytime emission rates estimated by inventory models, in order to evaluate their performance (for more details, see Fig. S3 in SI).

NEI (2014v1) provides daily emission rates on county level (available at the inventory supporting information), which, for comparison, were converted to EFs averaged by month, resulting in values of 4.5 $g_{NH3}/head_{Milk\ cow}/h$ in May and 4.1 $g_{NH3}/head_{Milk\ cow}/h$ in October for both counties (Kern and Tulare) (Fig. S4b in SI). The calculation of EFs was solely based on the number of milk cows, while heifers, bulls, and calves housed in dairy CAFOs were not included, in order to follow the NEI 2014 methodology. The use of a more refined model was hampered by limited knowledge of the studied CAFOs.

Because NH_3 emissions vary over the day, this needed to be considered when comparing with the SOF daytime-measured emissions. Diurnal emission profiles from modelling by (Zhu et al., 2015a) were used in our study, these were calculated by the EPA (J. Bash, Personal communication, 2020) for the respective locations and measured months (May and October 2019) (Fig. S4a in SI). The calculations were based on weather information from the WRF model 4.1.1 (weather research and forecasting) and the calculated data was given as monthly hourly fraction of NH_3 emissions $N_{met(t)}$.

Zhu et al. (2015a) obtain the diurnal emission pattern of NH_3 from the two equations below. The hourly fraction $N_{met(t)}$ (%) (Fig. S3 in SI) is first obtained from Eq. (3). After that, the hourly NH_3 emission rates (E_h (kg/h)) (Fig. S4a in SI) are obtained from Eq. (4), where E_m (kg/h) is monthly total emissions from the NEI 2014 v1.

$$N_{met(t)} = \frac{H_{(t)}/R_{a(t)}}{\sum_{t=1}^{n}\left(\frac{H_{(t)}}{R_{a(t)}}\right)} \quad (3)$$

$$E_h(t) = E_m N_{met}(t) \quad (4)$$

Here $R_{a(t)}$ (m/s) is atmospheric resistance at a specific time t, and $H_{(t)}$ is Henry's equilibrium constant, which is where the temperature is incorporated. Each hourly fraction is then divided by the sum of fractions of the whole month.

Fig. S4a in SI shows the estimated hourly NH_3 emission rates (E_h (kg/h)) for one of the dairies (SB05) in May and October, compared to modeled emission rates without the consideration of diurnal variation.

2.4.2. CH_4 emission rate comparison with the CARB inventory

For CH_4, we compared the average measured emission rates at the farm scale with emission rates obtained by the modeled California Air Resources Board (CARB) inventory. In the US, both national (U.S. Environmental Protection Agency, 2013) and the statewide (CARB, 2019b) CH_4 emission rates are derived from the methodology suggested by the International Panel for Climate Change (IPCC) (IPCC, 2006). The CH_4 inventory data (EFs) used in this study is specified for the climate and management conditions in the studied region by using EFs provided by CARB (CARB, 2019b) (Fig. S5 in SI). These estimations are divided into enteric fermentation and manure management EFs for each animal class (e.g., dairy cows, replacement heifers, and calves). For enteric emissions, the EF is multiplied by the number of animals at each life stage. For manure management practices, the EFs from each type of management have a different weight, which is based on CAFOs practices across the whole state of California. In the CARB inventory the following distribution for the manure from the dairy cows was assumed: 60% anaerobic lagoons, 10% daily spread, 20% liquid slurry, and 9% solid storage. In contrast, for heifers, 88% of manure treatment is assumed to be in dry lots, 11% daily spread, 1% pasture, and 1% liquid slurry. This approach is used because knowledge on the specific manure handling of the studied CAFOs was limited. Similarly, a recent study calculating CH_4 manure emissions in SJV, estimate that the largest percentage of the dairy manure (58–70%) was handled in anaerobic lagoons (Marklein et al., 2021). For the CAFOs with an anaerobic digester, the EF for this management were used instead of the anaerobic lagoons EF.

The comparisons between measurements and inventories for NH_3 was done with respect to time of the day, in contrast to CH_4, which was done for the annual average, because we assumed negligible diurnal variations. To obtain annual averages from the campaign measurements, the average emission rates were scaled to the full year. It should be noted that some of the farms were measured during two seasons, i.e. May and October (SB3, SB4, SB5, NB1 and NB2), while others were only measured once in May.

3. Results

3.1. NH_3 and CH_4 emission rates and emission factors

Fig. 2 shows the measurement approach used in this study demonstrated at dairy SB5, consisting of two nearby facilities housing 10,227 animals (mature cows, heifers, and bulls) corresponding to 12,750 livestock units (the detailed measured transects at SB5 are in Table S1 in SI). The obtained NH_3 columns (Fig. 2a and b) and ground concentrations of NH_3 and CH_4 (Fig. 2c and d) are shown along a measurement transect downwind of the CAFO. This measurement was complemented by upwind measurements. In May, the average emission and standard deviation from eight transects were 113.5 ± 49.2 kg_{NH3}/h, measured on two different days from 12:00 to 18:00, at an average wind speed of 2.34 ± 0.68 m/s and an average temperature of 28.11 ± 1.45 °C (Table S1 in SI). The plume ground concentration measurements gave an average

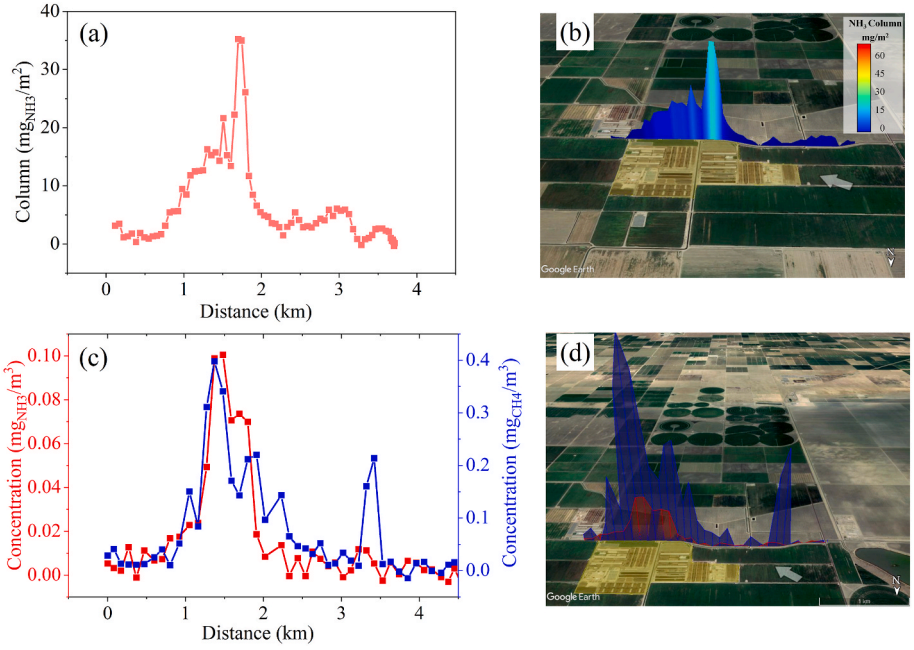

Fig. 2. Transects measured downwind of dairy SB05 on May 14th at 16:00. The measurements were obtained simultaneously, and the white arrow indicates wind direction. (a) NH_3 column. (b) Spatial location of the NH_3 column measurements. (c) Ground concentrations of NH_3 and CH_4. (d) Spatial location of NH_3 and CH_4 ground concentrations; the small CH_4 concentration plume on the far left side of the CAFO is likely due to emissions coming from a flooded area on the field. Map source: Google Earth.

NH_3:CH_4 ratio of 20.7 ± 8.9 g_{NH3}/g_{CH4}, resulting in an average CH_4 emission of 548 ± 137 kg_{CH4}/h. In October, NH_3 emission from SB05 averaged 130 ± 52 kg_{NH3}/h, and the NH_3:CH_4 ratio was 15 ± 9.1g_{NH3}/g_{CH4}, thereby giving a CH_4 emission of 873 ± 235 kg_{CH4}/h (Table S1 in SI).

Considering all CAFOs, average NH_3 emission rates varied between 31.9 kg_{NH3}/h and 191 kg_{NH3}/h (Tables S2 and SI), while average CH_4 emission rates varied between 155.3 kg_{CH4}/h and 873.6 kg_{CH4}/h (Tables S3 and SI). The highest NH_3 emissions were seen at WT4, which is one of the largest CAFOs, while for CH_4 the highest emission was seen at CAFO SB5 in the October campaign. The number of measurements per target facility was on average eight. The lowest emissions for both NH_3 and CH_4 were seen at ET1, which is the smallest dairy.

Fig. 3 shows the NH_3 and CH_4 EFs for the investigated 14 dairy CAFOs based on the measurements performed in May. EFs were obtained by normalizing the measured CAFOs emission rates by livestock unit. Around 40% of the dairies had an NH_3 EF higher than 10 g_{NH3}/LU/h (Fig. S6a in SI), the EFs median value corresponded to 9.8 g_{NH3}/LU/h and the 90th percentile of 12.1 g_{NH3}/LU/h (Table S2 in SI). EFs obtained by normalizing to only the number of mature animals were on average 16.4 ± 5.7 $g_{NH3}/head_{Mature\ cow}$/h or 18.9 ± 6.2 $g_{NH3}/head_{Milkcow}$/h. For CH_4, around 73% of the CAFOs had an EF below 50 g_{CH4}/LU/h and an EFs median of 34 g_{CH4}/LU/h (Fig. S6 in SI). For some of the dairies, such as NB2, the EF factors were rather high (Fig. 3b).

Comparison of the emissions measured in May and October for a subset of the CAFOs was done (Fig. 4). Average daytime temperatures during the individual measurements in each campaign were similar, i.e., 24 °C in May and 22 °C in October, respectively (Fig. S7 in SI). Average wind speeds during the individual measurement campaigns were higher in May (3.6 ± 1 m/s) than in October (2.8 ± 0.7 m/s). The results show that there was no difference in NH_3 emissions between the October and May campaigns (differences were within uncertainty levels), which could be expected from the fact that measurements were performed in seasons with similar average temperatures. The same is valid for the CH_4 measurements with the exception of CAFOs NB2 and SB4. One uncertainty that could not be accounted for was whether cattle numbers or CAFO management practices were the same during the two campaigns.

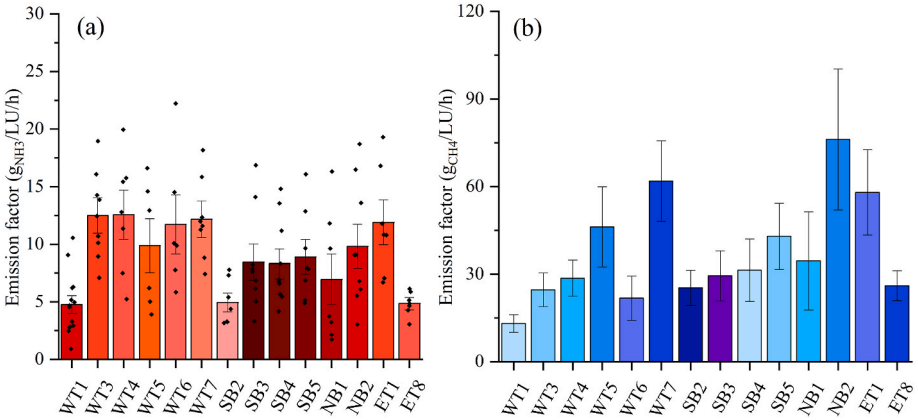

Fig. 3. (a) NH_3 emission factors (average and standard uncertainty (68% confidence limit)) and sampled transects (black dots). (b) CH_4 emission factors (average and standard uncertainty).

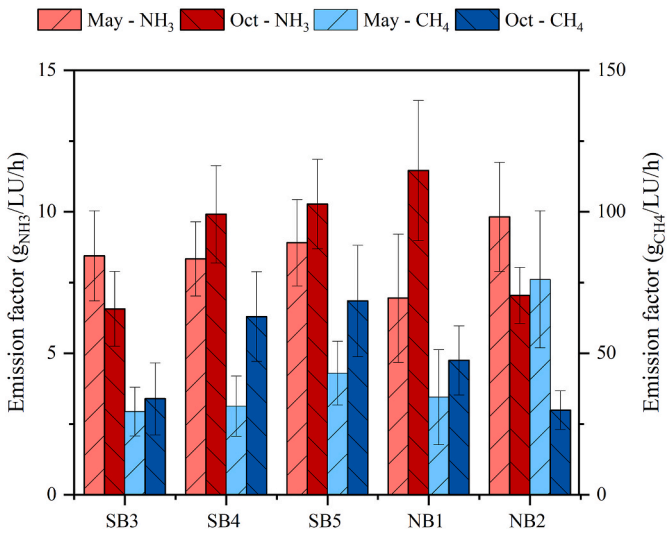

Fig. 4. EFs for five CAFOs during the October and May campaigns, and standard uncertainty.

4. Discussion

4.1. Measurement uncertainty

Errors in the SOF ammonia (NH_3) measurements were estimated per individual dairy (Table S4 in SI) following the GUM procedure (Joint Committee For Guides In Metrology, 2008), as illustrated in Table 3.

Uncertainty was dominated by the random error, directly estimated from the 1σ variability of the individual fluxes (or ratios) divided by the square root of the number of transects. In addition, systematic measurement errors, unchanged between measurements transects, were caused by the spectroscopic retrieval method, uncertainty in spectroscopic parameters, systematic inflow from upwind sources, and the assumed plume height. Here, the uncertainty related to the NH_3 cross-sections (Systematic error - strength of the cross-section) between 700 and 1200 cm^{-1} was obtained from Kleiner et al. (2003), which corresponds to 2% error. The retrieval error was obtained from the ratio between the standard deviation of the fitting residual, divided by square-root of the number of points, and the average NH_3 absorbance in 960–968 cm^{-1}. The wind speed error was obtained by the systematic discrepancy in the wind speed between the different heights intervals (0–50 m to 0–300 m). The last is a conservative estimate which, assumes that the plume height was estimated wrongly. The background error was estimated from any systematic differences in the upwind column values caused by the presence of interfering sources. The error was obtained by calculating the flux for the different baseline values, and comparing its average with the primarily estimate emission. Further, the average of the error from the different transects was used as the error value for the specific facility. Uncertainty was obtained by error propagation, taking the square root of the quadratic sum of the uncertainties as given in Table 3. The total estimated uncertainty for NH_3 median emission was 17% (range per facility of 11–32%) for 68% Confidence interval (CI) and 37% (range per facility of 23–76%) for 95% CI (Table 3 and Table S4 in SI).

Table 3
Measurement uncertainty for the direct and indirect flux calculations.

SOF/Direct Flux	
Systematic - Spectroscopic – strength of the cross-section NH_3	2 %[a]
Systematic - Spectroscopic - retrieval	4.4 %[a]
Systematic - Background errors (facility-specific)	1–14%
Systematic - Wind speed uncertainty in height	11–12%
Random - Measurement variability (facility-specific)	8–31%
Median standard uncertainty (68% confidence)	*17% (11–32%)*
Median expanded uncertainty (95% confidence)	*37% (23–76%)*
MeFTIR/Indirect flux	
Systematic - Spectroscopic – strength of the cross-section NH_3	0 %[a]
Systematic - Spectroscopic – strength of the cross-section CH_4	3%
Systematic - Spectroscopic – retrieval NH_3	0 %[a]
Systematic - Spectroscopic – retrieval CH_4	5.6%
Systematic - Sources mismatch (facility-specific)	5–41%
Systematic - SOF NH_3 uncertainty (facility-specific)	12–32%
Systematic - Background error – NH_3 (facility-specific)	1–10%
Systematic - Background error – CH_4 (facility-specific)	1–10%
Random - Ratios measurement variability (facility-specific)	5–36%
Median standard uncertainty (68% confidence)	*25% (19–49%)*
Median expanded uncertainty (95% confidence)	*53% (40–119%)*

[a] Some of the systematic spectroscopic errors for NH_3 will be cancelled out when doing the normalization (Eq. (2)) between SOF and MeFTIR.

The measurement error for CH_4 emissions includes uncertainty in both NH_3 emissions, as given above, and in estimating the NH_3-to-CH_4 ratio for the overall facility, since both are included when calculating the CH_4 emission. Uncertainty in the ratio is dominated by random uncertainty, estimated from the measured variability, although several systematic uncertainties are also important (Table 3 and Table S5 in SI). In particular, this includes the source misallocation error, which is caused by the fact that in some cases NH_3 and CH_4 are released at different distances away from the measurement position, and hence they are diluted differently. This error was assessed by Gaussian plume modeling (Fig. S8 in SI). Note that since the ratio is calculated from the integrated values across the measurement transect (Eq. (2)) it is mainly the difference in distance between source and measurement position along the wind that causes errors and not the sideways separation between the sources. Background error was similarly estimated for the concentration measurements of NH_3 and CH_4, while some of the systematic errors for NH_3 were cancelled out when doing the normalization between MeFTIR and SOF (Eq. (2)). The uncertainty on the CH_4 cross section was obtained from (Brown et al., 2003), while the reported error by MALT (Smith et al., 2011) was used as the CH_4 retrieval uncertainty. The median estimated uncertainty for CH_4 emissions was 25% (range per facility of 19–49%) for 68% CI and 53% (40–119%) for 95% CI (Table 3 and Table S5 in SI). Throughout the article, the authors adopted standard uncertainty (68% CI) in the data analysis, because it is more commonly used in scientific literature for this type of measurements (Johansson et al., 2014; Johnson et al., 2017).

4.2. Comparison of measured ammonia emission rates with other data

4.2.1. Measurement representativeness

NH_3 emissions from manure (feeding area, stall, or manure storage) are known to increase as a result of temperature, wind, and solar radiation (Hristov et al., 2011; Sun et al., 2015), consequently varying throughout different seasons (U.S. Environmental protection Agency, 2018). The measurements were carried out in May and October, and as can be seen in Fig. 4, the emissions are approximately the same during both periods and halfway between the modeled maximum and minimum emissions (Fig. S4b in SI). This is likely due to the fact that the average daily temperatures for both these months were close to the yearly average (May: 20 °C; Oct: 18.6 °C; Annual: 19.4 °C) (NOAA's National Weather Service, 2019). The diurnal model and the NEI inventory shows, that the NH_3 emissions should be 2% lower in October and 9% higher in May than the annual average, respectively (Fig. S4 in SI). Other variables as precipitation, humidity and solar radiation were not further evaluated, however, they should follow annual temperature trends, and therefore the measured months (October and May) would be close to the expected yearly average.

Studies that have measured NH_3 daily dynamics indicate that the difference between midday peak emissions and night-time lower emissions can vary by a factor of between two and five (Bjorneberg et al., 2009; Golston et al., 2020; Harper et al., 2009; Leytem et al., 2011; Sun

et al., 2015). As the SOF technique uses the sun as a light source, NH_3 measurements were carried out during the daytime and in sunny conditions. The NH_3 emission factors measured in this study showed a diurnal behavior with peak emissions at around 14:00 (Fig. 5b). In order to evaluate the diurnal variation of the measured NH_3 emissions, they were compared to modeled diurnal emissions, which were calculated using the average emission factor from the NEI inventory and a model for diurnal variation (Zhu et al., 2015a) provided by the US EPA (J. Bash, personal communication, 2020) (see section 2.4)). The single measured transect and modeled NH_3 emissions were normalized to the average CAFOs emissions of each measured facility, thus obtaining the emission variations. The modeled diurnal behavior for the specific measurement times is shown in Fig. 5a and b, while the full measurement period is in Fig. S4 in SI. It is evident that the average of the normalized SOF data and the model data agree rather well. Fig. S4 in SI shows the average inventory EF (straight line) and the modeled daily emission variations for May and October (bell shaped curve). The impact of diurnal emission variations caused in inventory and measurements comparisons has previously been pointed out by Lonsdale et al. (2017), who noted that the CARB inventory would be overestimated by a factor of 2.4 when compared to a single measurement at 13:00 local time.

The obtained NH_3 to CH_4 ratios, were normalized with the average ratio of each individual dairy value (Fig. 5c and d). The diurnal behavior of the NH_3 to CH_4 emission ratios followed the same diurnal trend as the NH_3 emissions. A similar diurnal pattern has been observed also in other studies (Eilerman et al., 2016; Golston et al., 2020; Miller et al., 2015). Most of the diurnal variation in the ratios are probably caused by changes in NH_3 emissions rather than CH_4, since temperature and solar insolation have relatively small impact on the emission on the latter (Arndt et al., 2018; Bjorneberg et al., 2009; Golston et al., 2020; Leytem et al., 2011; Sun et al., 2015). On average, 71% of the daytime variation in the ratio can be explained by NH_3 variations in October, based on the comparison between measured ratios and quantified fluxes, and 83% for the May data (Fig. 5). Multi-variable linear regression analyses of the measurement data (ratios and emission rates) versus ambient parameters (Table S6 in SI) shows significant correlations only for the time of the day.

4.2.2. Comparison of measured ammonia emission rates with inventory and other literature

On average, the measured NH_3 emissions were 28% higher in comparison to inventory estimates accounting for diurnal variations, using the model provided by Zhu et al. (2015a) (Fig. 6). This was not the case for all individual facilities, for example CAFO WT6 (Fig. 6). Excluding daily emission variations in the inventory emission rates, the measured emissions would instead be 71% higher. Some of the differences between measured and estimated emissions for specific facilities might be related to uncertainties in the numbers of animals, which can vary between the inspection day for the San Joaquim Valley pollution control district and the measurement day.

A comparison of emission factors at dairy cattle farms obtained in various studies is shown in Table 4. The EFs in this study are at the high end, consistent with that the SOF data (Kille et al., 2017) corresponds to daytime values, as discussed above, and the same tendency can also be seen in other daytime studies. By assuming the modeled diurnal pattern described above (Zhu et al., 2015a), the measured EF factors were converted to daily averages corresponding to 3.0 g_{NH3}/h/LU/in May and to 4.2 g_{NH3}/h/LU in October, respectively; hence in better agreement with some of the other studies in Table 4. Additionally, according to recent studies, NH_3 emissions measured close to ground level might be underestimated due to NH_3 deposition or missampling of the concentrated part of the plume. The plume might be located lofted, which would not affect SOF measurements, since it measures whole air columns concentrations (Lassman et al., 2020), differently from ground measurements only. It is relevant to highlight that most of the farms were measured under similar wind speed conditions, except WT06 and WT04, measured at averaged higher wind speeds, which could partially explain the high emission factors observed compared to inventory estimates.

4.3. Comparison of the measured CH_4 emission rates with other data

The measured farm-scale CH_4 emissions were on average 60% higher than those modeled by inventories. For the five CAFOs that were measured both in May and October the average difference drops to 40%. The measured CH_4 emissions are associated with greater uncertainties than the NH_3 fluxes, and the variability between individual facilities

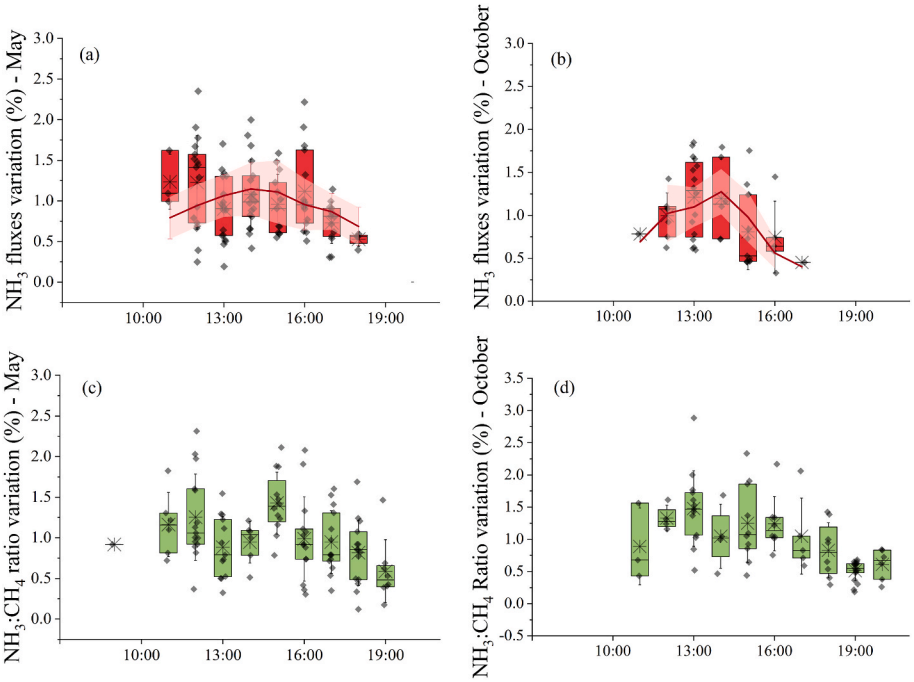

Fig. 5. Variation of NH_3 emissions (a, b) and NH_3:CH_4 ratios (c, d) versus time of the day for all CAFOs (time specific by average) and classified according to the measured period. Solid lines in Figures a and b correspond to the average of the modeled values from the same period as the measurements. In the box plot, the average is indicated by the star-shaped symbol. The diamond symbols correspond to each measured transect. The upper box represented the 75% percentile, while the lower corresponds to 25% percentile. The whiskers show the standard deviation.

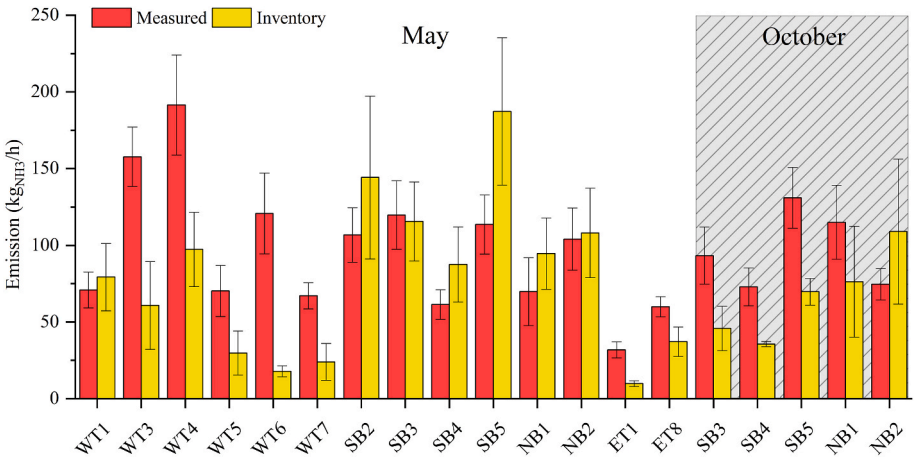

Fig. 6. Comparison of measured NH_3 emissions (average and standard uncertainty), and modeled day time emissions (average and standard deviation from hourly emissions), using NEI 2014 and (Zhu et al., 2015a)(average and standard deviation).

Table 4
Average emission factors at CAFOs for NH_3 and CH_4 with corresponding standard uncertainties. In addition, NH_3:CH_4 ratios from other studies are illustrated.

Farm	Period	Method/Instrument	NH_3 (g/h/LU) [k]	NH_3 (g/h/head)	CH_4 (g/h/LU)	CH_4 (g/h/head) [l]	NH_3:CH_4 g/g
Present study dairy, CAFO (California)	Spring and autumn (Day-time)	SOF and MeFTIR	9.0 ± 2.6	16.8 ± 5.5	40.1 ± 17.8	74.0 ± 32.8	21
Average farm NEI (NH_3) and CARB inventory (CH_4)[m]	Yearly	Inventory	6.7–6.8		30.7		
Dairy, CAFO (Colorado)[a]	August (Day-time)	SOF		11.4 ± 3.4			
Dairy, CAFO (Colorado)[b]	Summer, winter, spring, autumn	Cavity Ring spectroscopy					14–17
Dairy, CAFO (California)[c]	Winter (January)	Open-Path (WMS, Licor)					14 ± 3
Dairy farm (California)[d]	Winter and summer	Open path/Inverse dispersion modeling			26.0 ± 7.4 (Winter) 58.9 ± 10.5 (Summer)		
Dairy farm (Washington)[e]	Yearly model	DOAS, Tracer ratio flux		4.6			
Dairy CAFO (Idaho)[f]	Summer, winter, spring, autumn	Open-path FTIR/Inverse Dispersion modeling	8.1 1.2	10.4 1.7	17.1 5.3	22.9 8.3	12–90
Dairy CAFOs (California)[g]	Summer (June)	Airborne/surface (AMOG/MISTIR)		38		76	52
Dairy CAFO (Idaho)[h]	Whole year (Monthly)	Open-path/Inverse dispersion method	4.9	6.3	45.1	57.9	2–10
Dairy CAFO (Colorado)[i]	Summer	Tildas, Licor and others/modeled emissions	5.3 ± 0.5		39.3 ± 3.9		40
Dairy farm(Canada)[j]	Spring and autumn	Open-path/inverse dispersion modeling				20.7 ± 1.2 8.8 ± 2.2	37

[a] Kille et al., 2017.
[b] Eilerman et al., 2016.
[c] Miller et al., 2015.
[d] Arndt et al., 2018.
[e] Rumburg et al., 2008.
[f] Bjorneberg et al., 2009.
[g] Leifer et al., 2018.
[h] Leytem et al., 2011.
[i] Golston et al., 2020.
[j] VanderZaag et al., 2014.
[k] Livestock unit (LU), 1 LU = 500 kg of body weight.
[l] head of dairy cows only.
[m] U.S. Environmental protection Agency, 2018, CARB, 2019b.

were relatively high (Fig. 7). The uncertainty is especially large for some CAFOs, e.g., NB1-May, a result of the combined SOF and ratios' large measurement variability.

The inventory values agree with the measurements in 9 out of 19 measurements when considering the 68% CI (Fig. 7).The measurements are at the high end of the values reported in other studies (Table 4). Recent studies have found a good correlation between measured CH_4 and inventory (Arndt et al., 2018; Golston et al., 2020).

Most (75%) of the measured NH_3:CH_4 ground concentration ratios (n = 205) were below 25 g_{NH3}/g_{CH4} (Fig. S6b in SI). Differences within CAFOs are likely a reflection of differences in management or measurement time. A few observed ratios were larger than 80 g_{NH3}/g_{CH4}, likely due to specific short-term activities, e.g., the mixing of solid manure piles, which could be observed from the CAFO fence line. The ratios obtained are comparable to results from recent studies carried out in the same area or at the same type of facility (Eilerman et al., 2016; Miller et al., 2015). There are differences when compared to some other studies (Bjorneberg et al., 2009; Kille et al., 2019; Leifer et al., 2018), but we believe this is mostly due to different seasons or manure management.

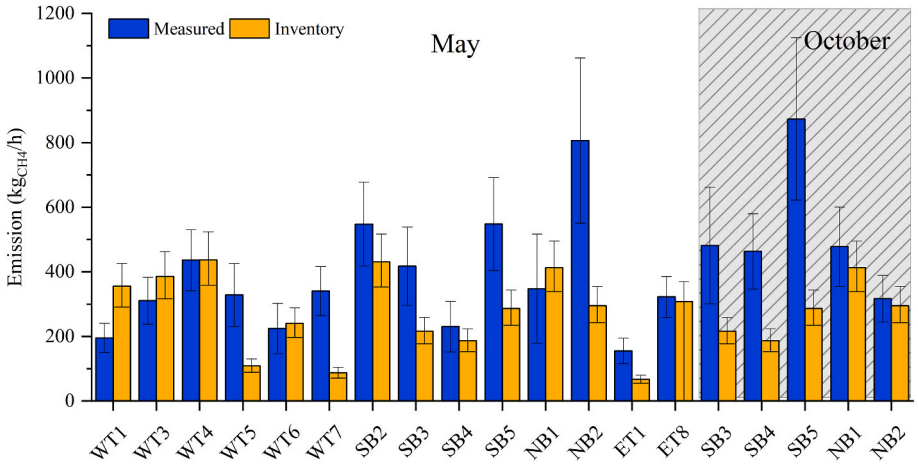

Fig. 7. Comparison of measured CH_4 emissions (average and standard uncertainty) and CARB inventory annual emissions (average and CI 95%) (U.S. Environmental Protection Agency, 2013).

4.3.1. *Factors affecting CH_4 emissions*

While NH_3 emissions are consistently reported to vary during the day, this is not the case for CH_4 emissions. Arndt et al. (2018) noted a small increase during rumination time, Leytem et al. (2011) found larger variations between day and night, Golston et al. (2020) and Sun et al. (2015) found an increase in emissions at the end of the day, while others did not observe any clear pattern at all (Bjorneberg et al., 2009). For CH_4 emissions, seasonal variations have also been reported (Bjorneberg et al., 2009; Leytem et al., 2011); however, since the campaign months of May and October have temperatures close to the annual average, our measurements should also be close to annual averaged emission values.

In this study, we lack detailed knowledge about manure management practices at the CAFOs that can influence CH_4 emissions, such as manure management, storage time, and animal feeding. However, a rough assessment of the manure practices at the individual facilities was done during the campaigns by studying maps and making visual observations, e.g., making it possible to identify farms with and without a manure lagoon cover, which enables the facility to collect the CH_4 produced in lagoons and use the gas as an energy source. In total, 5 of the measured CAFOs used this system. Noteworthy here is that these farms did not emit significantly less than those without a cover (Fig. 8). Uncertainties in terms of animal numbers or the measurements may have contributed to concealing any differences. An alternative explanation is that even though we did observe the presence of a lagoon cover, we lacked information regarding whether the system was actually operational. For example, observation of high CH_4 peaks persistently correlated to the digesters. Additionally, two of the farms had their systems recently built, thus raising doubts about whether or not they were already operational.

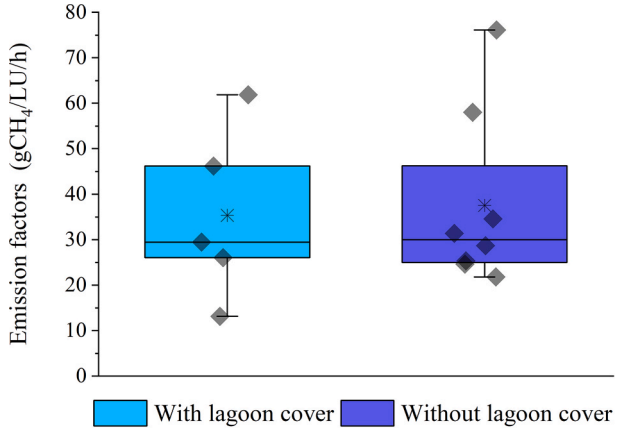

Fig. 8. Comparison of CH_4 emissions from CAFOs with and without a lagoon cover. The mean is represented by the square symbol, the median by the horizontal solid line, the lower part of the box shows the 25th percentile while the upper part is the 75th percentile.

4.3.2. *Comparison of measured CH_4 emissions and previous measurements, using other techniques*

Some of the farms in this study were previously measured for airborne CH_4 emissions by Scientific Aviation (Thompson et al., 2019), as illustrated in Fig. 9. The approach used by Scientific Aviation comprises a mass balance calculation, based on Gaussian law. The aircraft flies in circles around the facility, from the minimum safe height to above the plume height (Conley et al., 2017).

These measurements were carried out over four campaigns in 2018 and 2019, and the last one coincided in time with this study, as indicated in Fig. 9. For sites SB2 and SM1, measurements were done on the same day or within a few days. The error bars in the Scientific Aviation data correspond to measurement uncertainty. As evidence herein, the two datasets overlap reasonably well, given the measurement uncertainties, with the exception of ET8. Note that the latter airborne measurement

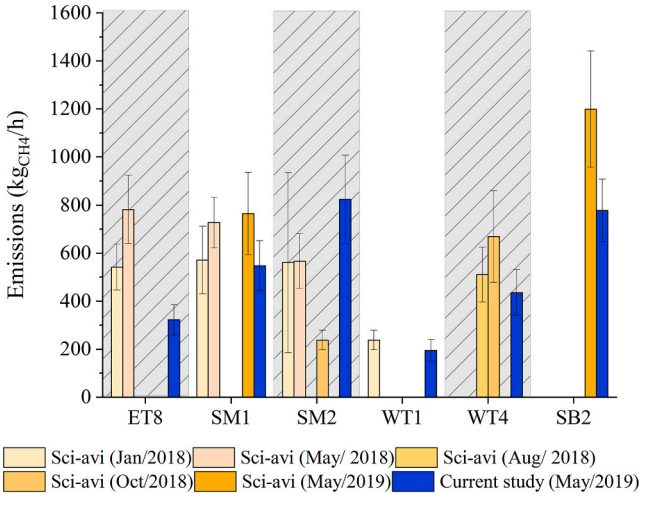

Fig. 9. Comparison of CH_4 emission rates measured by Scientific Aviation using a mass balance approach and SOF (present study) (average and standard uncertainty). The farms compared here are ET8, WT1, WT4, SB2, and two other from Madera County, which were not included in the inventory analysis. SB2 measurements were done on the same day.

was carried out one year before the present study. The advantage of the indirect flux technique over the airborne mass flux approach is its higher spatial resolution and, consequently, the ability to measure an individual facility more easily, although both approaches have a limitation relating to the measurement period, because they require specific weather conditions.

5. Conclusions

Several optical methods, i.e., solar occultation flux (SOF) and MeFTIR, were used to quantify ammonia (NH_3) and methane (CH_4) emissions, respectively, at dairy CAFOs in the San Joaquin Valley, California, United States. The measurement uncertainty of NH_3 flux by SOF for the measured CAFOs was estimated to a median value of 17% for 68% CI, and the largest error sources were measurement variability (random error) and wind speed uncertainty. When comparing daytime emissions of NH_3 measured by SOF with inventory data, the former yields 71% higher emission values than the latter, primarily driven by the fact that the emissions are affected by temperature and solar insolation. When taking diurnal variations in these environmental factors into account the difference is lowered to 28%. In addition, when comparing the daytime emission results from SOF to other studies in the literature, the former are at the high end, since most of the other studies include both day and night contributions.

The CH_4 emission measurements have larger uncertainties than the NH_3 measurements (25% for 68% CI, and 53% for 95% CI). The measured emissions are 60% higher than the CARB inventory, and the values are towards the high end when compared to other studies in the literature. An uncertainty in this study is in the lack of detailed knowledge about management practices in the measured facilities. From visual observations, it is estimated that 35% of the CAFOs had covered manure lagoons. However, this practice was not observed to abate the emissions. The obtained CH_4 emissions in this study correspond reasonably well with airborne measurements done using a mass balance approach at six of the studied CAFOs, indicating that our CH_4 results were consistent with other measurement approaches.

Complementary measurements during night periods or in different seasons could provide a better understanding of emissions dynamics. The methods described herein offer a suitable approach for monitoring emissions from CAFOs, as they can cover several facilities in a short time period, without being expensive or labor-intensive.

CRediT authorship contribution statement

N.T. Vechi: Conceptualization, Writing – original draft, Writing – review & editing, Data curation, Formal analysis, Investigation. **J. Mellqvist:** Conceptualization, Writing – review & editing, Methodology, Data curation, Funding acquisition, Supervision. **J. Samuelsson:** Methodology, Data curation, Project administration. **B. Offerle:** Methodology, Data curation, Formal analysis. **C. Scheutz:** Conceptualization, Formal analysis, Funding acquisition, Writing – review & editing, Supervision.

Declaration of competing interest

The authors declare that they have no known competing financial interests or personal relationships that could have appeared to influence the work reported in this paper.

Data availability

Data will be made available on request.

Acknowledgments

This data was collected under sponsorship from CARB, contract 17RD021 "Characterization of Air Toxics and GHG Emission Sources and their Impacts on Community-Scale Air Quality Levels in Disadvantaged Communities" by FluxSense Inc. We are especially thankful to Jesse Bash from the U.S. Environmental Protection Agency for providing us with the ammonia diurnal normalized profiles.

Appendix A. Supplementary data

Supplementary data to this article can be found online at https://doi.org/10.1016/j.atmosenv.2022.119448.

References

American Jersey Cattle Association, 2015. A Quality Heifer. Productive Life in the Industry.

Arndt, C., Leytem, A.B., Hristov, A.N., Zavala-Araiza, D., Cativiela, J.P., Conley, S., Daube, C., Faloona, I., Herndon, S.C., 2018. Short-term methane emissions from 2 dairy farms in California estimated by different measurement techniques and US Environmental Protection Agency inventory methodology: a case study. J. Dairy Sci. 101, 11461–11479. https://doi.org/10.3168/jds.2017-13881.

Bjorneberg, D.L., Leytem, a B., Westermann, D.T., Griffiths, P.R., Shao, L., Pollard, M.J., 2009. Measurement of atmospheric ammonia, methane, and nitrous oxide at a concentrated dairy production facility in southern Idaho using open-path FTIR spctrometry. Transcations Am. Soc. Agric. Biol. Eng. 52, 1749–1756. https://doi.org/10.13031/2013.29137.

Brodeur, J.J., Warland, J.S., Staebler, R.M., Wagner-Riddle, C., 2009. Technical note: laboratory evaluation of a tunable diode laser system for eddy covariance measurements of ammonia flux. Agric. For. Meteorol. 149, 385–391. https://doi.org/10.1016/j.agrformet.2008.08.009.

Brown, L.R., Benner, D.C., Champion, J.P., Devi, V.M., Fejard, L., Gamache, R.R., Gabard, T., Hilico, J.C., Lavorel, B., Loete, M., Mellau, G.C., Nikitin, A., Pine, A.S., Predoi-Cross, A., Rinsland, C.P., Robert, O., Sams, R.L., Smith, M.A.H., Tashkun, S. A., Tyuterev, V.G., 2003. Methane line parameters in HITRAN. J. Quant. Spectrosc. Radiat. Transf. 82, 219–238. https://doi.org/10.1016/S0022-4073(03)00155-9.

CARB, 2019a. CH4 [WWW Document]. URL. https://ww3.arb.ca.gov/cc/inventory/background/ch4.htm, 8.18.20.

CARB, 2019b. Greenhouse gas emissions inventory - query results [WWW Document]. Greenh. Gas Emiss. Invent. Summ. [2000 - 2017]. URL. https://www.arb.ca.gov/app/ghg/2000_2017/ghg_sector_data.php, 9.2.20.

Conley, S., Faloona, I., Mehrotra, S., Suard, M., Lenschow, D.H., Sweeney, C., Herndon, S., Schwietzke, S., Pétron, G., Pifer, J., Kort, E.A., Schnell, R., 2017. Application of Gauss's theorem to quantify localized surface emissions from airborne measurements of wind and trace gases. Atmos. Meas. Tech. 10, 3345–3358. https://doi.org/10.5194/amt-10-3345-2017.

Delre, A., Mønster, J., Samuelsson, J., Fredenslund, A.M., Scheutz, C., 2018. Emission quantification using the tracer gas dispersion method: the influence of instrument, tracer gas species and source simulation. Sci. Total Environ. 634, 59–66. https://doi.org/10.1016/j.scitotenv.2018.03.289.

Eilerman, S.J., Peischl, J., Neuman, J.A., Ryerson, T.B., Aikin, K.C., Holloway, M.W., Zondlo, M.A., Golston, L.M., Pan, D., Floerchinger, C., Herndon, S., 2016. Characterization of ammonia, methane, and nitrous oxide emissions from concentrated animal feeding operations in northeastern Colorado. Environ. Sci. Technol. 50, 10885–10893. https://doi.org/10.1021/acs.est.6b02851.

European standard, 2022. EN 17628:2022 [WWW Document]. URL. https://www.sis.se/api/docu ment/preview/80034943/.

Golston, L.M., Pan, D., Sun, K., Tao, L., Zondlo, M.A., Eilerman, S.J., Peischl, J., Neuman, J.A., Floerchinger, C., 2020. Variability of ammonia and methane emissions from animal feeding operations in northeastern Colorado. Environ. Sci. Technol. 54, 11015–11024. https://doi.org/10.1021/acs.est.0c00301.

Griffith, D.W.T., 1996. Synthetic calibration and quantitative analysis of gas-phase FT-IR spectra. Appl. Spectrosc. 50, 59–70. https://doi.org/10.1366/0003702963906627.

Harper, L.A., Flesch, T.K., Powell, J.M., Coblentz, W.K., Jokela, W.E., Martin, N.P., 2009. Ammonia emissions from dairy production in Wisconsin. J. Dairy Sci. 92, 2326–2337. https://doi.org/10.3168/jds.2008-1753.

Harris, T.D., Smith, V.H., Graham, J.L., Waa, D.B.V. de, Tedesco, L.P., Clercin, N., 2016. Combined effects of nitrogen to phosphorus and nitrate to ammonia ratios on cyanobacterial metabolite concentrations in eutrophic Midwestern USA reservoirs. Inl. Waters 6, 199–210. https://doi.org/10.5268/IW-6.2.938.

Hristov, A.N., Hanigan, M., Cole, A., Todd, R., McAllister, T.A., Ndegwa, P.M., Rotz, A., 2011. Review: ammonia emissions from dairy farms and beef feedlots. Can. J. Anim. Sci. 91, 1–35. https://doi.org/10.4141/CJAS10034.

Hristov, A.N., Harper, M., Meinen, R., Day, R., Lopes, J., Ott, T., Venkatesh, A., Randles, C.A., 2017. Discrepancies and uncertainties in bottom-up gridded inventories of livestock methane emissions for the contiguous United States. Environ. Sci. Technol. 51, 13668–13677. https://doi.org/10.1021/acs.est.7b03332.

Hristov, A.N., Kebreab, E., Niu, M., Oh, J., Bannink, A., Bayat, A.R., Boland, T.M., Brito, A.F., Casper, D.P., Crompton, L.A., Dijkstra, J., Eugène, M., Garnsworthy, P.C., Haque, N., Hellwing, A.L.F., Huhtanen, P., Kreuzer, M., Kuhla, B., Lund, P., Madsen, J., Martin, C., Moate, P.J., Muetzel, S., Muñoz, C., Peiren, N., Powell, J.M., Reynolds, C.K., Schwarm, A., Shingfield, K.J., Storlien, T.M., Weisbjerg, M.R., Yáñez-Ruiz, D.R., Yu, Z., 2018. Symposium review: uncertainties in enteric methane

inventories, measurement techniques, and prediction models. J. Dairy Sci. 6655–6674. https://doi.org/10.3168/jds.2017-13536.
IPCC, 2006. IPCC Guidelines for National Greenhouse Gas Inventories, Agriculture, Forestry and Other Land Use, Prepared by the National Greenhouse Gas Inventories Programme. CIGES, Japan.
IPCC, 2021. Climate Change 2021: the Physical Science Basis.. Contribution of Working Group I to the Sixth Assessment Report of the Intergovernmental Panel on Climate Change. Cambridge University Press, Cambridge, United Kingdom and New York, NY, USA.
Johansson, J., 2016. Optical Remote Sensing of Industrial Gas Emission Fluxes. Chalmer University of Technology.
Johansson, J., Mellqvist, J., Samuelsson, J., Offerle, B., Lefer, B., Rappenglück, B., Flynn, J., Yarwood, G., 2014. Emission measurements of alkenes, alkanes, SO2 and NO2 from stationary sources in southeast Texas over a 5 year period using SOF and Mobile DOAS. J. Geophys. Res. 1–8. https://doi.org/10.1002/2013JD021350 (Received).
Johnson, M.R., Tyner, D.R., Conley, S., Schwietzke, S., Zavala-Araiza, D., 2017. Comparisons of airborne measurements and inventory estimates of methane emissions in the alberta upstream oil and gas sector. Environ. Sci. Technol. 51, 13008–13017. https://doi.org/10.1021/acs.est.7b03525.
Joint Committee For Guides In Metrology, 2008. Evaluation of measurement data - guide to the expression of uncertainty in measurement. Int. Organ. Stand. Geneva 50, 134. ISBN.
Kihlman, M., 2005. Application of Solar FTIR Spectroscoy for Quantingfying Gas Emissions. Chalmers University of Technology, Gothenburg, Sweden.
Kille, N., Baidar, S., Handley, P., Ortega, I., Sinreich, R., Cooper, O.R., Hase, F., Hannigan, J.W., Pfister, G., Volkamer, R., 2017. The CU mobile Solar Occultation Flux instrument: structure functions and emission rates of NH3, NO2 and C2H6. Atmos. Meas. Tech. 10, 373–392. https://doi.org/10.5194/amt-10-373-2017.
Kille, N., Chiu, R., Frey, M., Hase, F., Sha, M.K., Blumenstock, T., Hannigan, J.W., Orphal, J., Bon, D., Volkamer, R., 2019. Separation of methane emissions from agricultural and natural gas sources in the Colorado front range. Geophys. Res. Lett. 46, 3990–3998. https://doi.org/10.1029/2019GL082132.
Kleiner, I., Tarrago, G., Cottaz, C., Sagui, L., Brown, L.R., Poynter, R.L., Pickett, H.M., Chen, P., Pearson, J.C., Sams, R.L., Blake, G.A., Matsuura, S., Nemtchinov, V., Varanasi, P., Fusina, L., Di Lonardo, G., 2003. NH3 and PH3 line parameters: the 2000 HITRAN update and new results. J. Quant. Spectrosc. Radiat. Transf. 82, 293–312. https://doi.org/10.1016/S0022-4073(03)00159-6.
Lassman, W., Collett, J.L., Ham, J.M., Yalin, A.P., Shonkwiler, K.B., Pierce, J.R., 2020. Exploring new methods of estimating deposition using atmospheric concentration measurements: a modeling case study of ammonia downwind of a feedlot. Agric. For. Meteorol. 290 https://doi.org/10.1016/j.agrformet.2020.107989.
Leifer, I., Melton, C., Tratt, D.M., Buckland, K.N., Chang, C.S., Frash, J., Hall, J.L., Kuze, A., Leen, B., Clarisse, L., Lundquist, T., Van Damme, M., Vigil, S., Whitburn, S., Yurganov, L., 2018. Validation of mobile in situ measurements of dairy husbandry emissions by fusion of airborne/surface remote sensing with seasonal context from the Chino Dairy Complex. Environ. Pollut. 242, 2111–2134. https://doi.org/10.1016/j.envpol.2018.03.078.
Leifer, I., Melton, C., Tratt, D.M., Buckland, K.N., Clarisse, L., Coheur, P., Frash, J., Gupta, M., Johnson, P.D., Leen, J.B., Van Damme, M., Whitburn, S., Yurganov, L., 2017. Remote sensing and in situ measurements of methane and ammonia emissions from a megacity dairy complex: chino, CA. Environ. Pollut. 221, 37–51. https://doi.org/10.1016/j.envpol.2016.09.083.
Lelieveld, J., Evans, J.S., Fnais, M., Giannadaki, D., Pozzer, A., 2015. The contribution of outdoor air pollution sources to premature mortality on a global scale. Nature 525, 367–371. https://doi.org/10.1038/nature15371.
Leytem, A.B., Dungan, R.S., Bjorneberg, D.L., Koehn, A.C., 2011. Emissions of ammonia, methane, carbon dioxide, and nitrous oxide from dairy cattle housing and manure management systems. J. Environ. Qual. 40, 1383. https://doi.org/10.2134/jeq2009.0515.
Locker, I., Woodward, A., 2010. Introducing the New ZephIR 300. Wind. Int.
Lonsdale, C.R., Hegarty, J.D., Cady-pereira, K.E., Alvarado, M.J., Henze, D.K., Turner, M. D., Capps, S.L., Nowak, J.B., Neuman, J.A., Middlebrook, A.M., Bahreini, R., Murphy, J.G., Markovic, M.Z., Vandenboer, T.C., Russell, L.M., 2017. Modeling the diurnal variability of agricultural ammonia in Bakersfield. In: California , during the CalNex campaign, pp. 2721–2739. https://doi.org/10.5194/acp-17-2721-2017, 3.
Marklein, A.R., Meyer, D., Fischer, M.L., Jeong, S., Rafiq, T., Carr, M., Hopkins, F.M., 2021. Facility-scale inventory of dairy methane emissions in California: implications for mitigation. Earth Syst. Sci. Data 13, 1151–1166. https://doi.org/10.5194/essd-13-1151-2021.
Mellqvist, J., Samuelsson, J., Andersson, P., Brohede, S., Isoz, O., Ericsson, M., 2017. Using Solar Occultation Flux and Other Optical Remote Sensing Methods to Measure VOC Emissions from a Variety of Stationary Sources in the South Coast Air Basin.
Mellqvist, J., Samuelsson, J., Johansson, J., Rivera, C., Lefer, B., Alvarez, S., Jolly, J., 2010. Measurements of industrial emissions of alkenes in Texas using the solar occultation flux method. J. Geophys. Res. 115, D00F17. https://doi.org/10.1029/2008JD011682.
Mellqvist, J., Samuelsson, J., Rivera, C., 2007. HARC Project H-53 Measurements of industrial emissions of VOCs , NH 3 , NO 2 and SO 2 in Texas using the Solar Occultation Flux method and mobile. DOAS 2007, 1–69.
Miller, B.R., Dlugokencky, E.J., Eluszkiewicz, J., Fischer, M.L., Janssens-maenhout, G., 2013. Anthropogenic emissions of methane in the United States 110, 20018–20022. https://doi.org/10.1073/pnas.1314392110/-/DCSupplemental.www.pnas.org/cgi/doi/10.1073/pnas.1314392110.
Miller, D.J., Sun, K., Tao, L., Pan, D., Zondlo, M.A., Nowak, J.B., Liu, Z., Diskin, G., Sachse, G., Beyersdorf, A., Ferrare, R., Scarino, A.J., 2015. Ammonia and methane dairy emission plumes in the San Joaquin valley of California from individual feedlot to regional scales. J. Geophys. Res. 120, 9718–9738. https://doi.org/10.1002/2015JD023241.
Monson, J., Chigbu, C., Tang, L., Goss, S., 2017. California Dairy Statistics Annual: 2017 Data 18.
Ngwabie, N.M., Jeppsson, K.H., Gustafsson, G., Nimmermark, S., 2011. Effects of animal activity and air temperature on methane and ammonia emissions from a naturally ventilated building for dairy cows. Atmos. Environ. 45, 6760–6768. https://doi.org/10.1016/j.atmosenv.2011.08.027.
NOAA's National Weather Service, 2019. Bakersfield Climate [WWW Document].
Nowak, J.B., Neuman, J.A., Bahreini, R., Middlebrook, A.M., Holloway, J.S., McKeen, S. A., Parrish, D.D., Ryerson, T.B., Trainer, M., 2012. Ammonia sources in the California South Coast Air Basin and their impact on ammonium nitrate formation. Geophys. Res. Lett. 39, 6–11. https://doi.org/10.1029/2012GL051197.
Owen, J.J., Silver, W.L., 2015. Greenhouse gas emissions from dairy manure management: a review of field-based studies. Global Change Biol. 21, 550–565. https://doi.org/10.1111/gcb.12687.
Rennie, T.J., Gordon, R.J., Smith, W.N., VanderZaag, A.C., 2018. Liquid manure storage temperature is affected by storage design and management practices-A modelling assessment. Agric. Ecosyst. Environ. 260, 47–57. https://doi.org/10.1016/j.agee.2018.03.013.
Rothman, L.S., Jacquemart, D., Barbe, A., Benner, D.C., Birk, M., Brown, L.R., Carleer, M. R., Chackerian, C., Chance, K., Coudert, L.H., Dana, V., Devi, V.M., Flaud, J.M., Gamache, R.R., Goldman, A., Hartmann, J.M., Jucks, K.W., Maki, A.G., Mandin, J.Y., Massie, S.T., Orphal, J., Perrin, A., Rinsland, C.P., Smith, M.A.H., Tennyson, J., Tolchenov, R.N., Toth, R.A., Vander Auwera, J., Varanasi, P., Wagner, G., 2005. The HITRAN 2004 molecular spectroscopic database. J. Quant. Spectrosc. Radiat. Transf. 96, 139–204. https://doi.org/10.1016/j.jqsrt.2004.10.008.
Rumburg, B., Mount, G.H., Filipy, J., Lamb, B., Westberg, H., Yonge, D., Kincaid, R., Johnson, K., 2008. Measurement and modeling of atmospheric flux of ammonia from dairy milking cow housing. Atmos. Environ. 42, 3364–3379. https://doi.org/10.1016/j.atmosenv.2007.05.042.
Samuelsson, J., Delre, A., Tumlin, S., Hadi, S., Offerle, B., Scheutz, C., 2018. Optical technologies applied alongside on-site and remote approaches for climate gas emission quantification at a wastewater treatment plant. Water Res. 131, 299–309. https://doi.org/10.1016/j.watres.2017.12.018.
Sharpe, S.W., Johnson, T.J., Sams, R.L., Chu, P.M., Rhoderick, G.C., Johnson, P.A., 2004. Gas-phase databases for quantitative infrared spectroscopy. Appl. Spectrosc. 58, 1452–1461. https://doi.org/10.1366/0003702042641281.
Smith, D.A., Harris, M., Coffey, A.S., Park, T., 2006. Wind test site in høvsøre. Evaluation 87–93.
Smith, T.E.L., Wooster, M.J., Tattaris, M., Griffith, D.W.T., 2011. Absolute accuracy and sensitivity analysis of OP-FTIR retrievals of CO2, CH4 and CO over concentrations representative of "clean air" and "polluted plumes.". Atmos. Meas. Tech. 4, 97–116. https://doi.org/10.5194/amt-4-97-2011.
Sun, K., Tao, L., Miller, D.J., Zondlo, M.A., Shonkwiler, K.B., Nash, C., Ham, J.M., 2015. Open-path eddy covariance measurements of ammonia fluxes from a beef cattle feedlot. Agric. For. Meteorol. 213, 193–202. https://doi.org/10.1016/j.agrformet.2015.06.007.
The Pennsylvania State University, 2017. Growth charts for dairy heifers [WWW Document]. URL. https://extension.psu.edu/growth-charts-for-dairy-heifers, 6.16.21.
Thompson, C., Stockwell, C., Smith, M., Conley, S., 2019. Statewide Airborne Methane Emissions Measurement Survey - Final Summary Report 69.
U.S. Environmental protection Agency, 2018. National Emissions Inventory 2014. North Carolina.
U.S. Environmental Protection Agency, 2013. 2013 GHGI Annex.
US-EPA, 2012. Chapter 2 - AFOs and CAFOs. In: NPDES Permit Writers' Manual for CAFOs, pp. 1–16.
USDA, 2021. Usda ers - dairy data [WWW Document]. URL. https://www.ers.usda.gov/data-products/dairy-data/, 4.4.21.
VanderZaag, A.C., Flesch, T.K., Desjardins, R.L., Baldé, H., Wright, T., 2014. Measuring methane emissions from two dairy farms: seasonal and manure-management effects. Agric. For. Meteorol. 194, 259–267. https://doi.org/10.1016/j.agrformet.2014.02.003.
Zhu, L., Henze, D., Bash, J., Jeong, G.R., Cady-Pereira, K., Shephard, M., Luo, M., Paulot, F., Capps, S., 2015a. Global evaluation of ammonia bidirectional exchange and livestock diurnal variation schemes. Atmos. Chem. Phys. 15, 12823–12843. https://doi.org/10.5194/acp-15-12823-2015.
Zhu, L., Henze, D.K., Bash, J.O., Cady-Pereira, K.E., Shephard, M.W., Luo, M., Capps, S. L., 2015b. Sources and impacts of atmospheric NH3: current understanding and frontiers for modeling, measurements, and remote sensing in North America. Curr. Pollut. Rep. 1, 95–116. https://doi.org/10.1007/s40726-015-0010-4.